ACS APPLIED MATERIALS & INTERFACES

Research Article

www.acsami.org

Switchable Adhesion in Vacuum Using Bio-Inspired Dry Adhesives

Julia Purtov,[†,‡,§] Mareike Frensemeier,[†,‡,§] and Elmar Kroner*[,‡,§]

[†]Department of Materials Science and Engineering, Saarland University, Campus D2 2, 66123 Saarbrücken, Germany

[‡]INM – Leibniz Institute for New Materials, Campus D2 2, 66123 Saarbrücken, Germany

Supporting Information

ABSTRACT: Suction based attachment systems for pick and place handling of fragile objects like glass plates or optical lenses are energy-consuming and noisy and fail at reduced air pressure, which is essential, e.g., in chemical and physical vapor deposition processes. Recently, an alternative approach toward reversible adhesion of sensitive objects based on bioinspired dry adhesive structures has emerged. There, the switching in adhesion is achieved by a reversible buckling of adhesive pillar structures. In this study, we demonstrate that these adhesives are capable of switching adhesion not only in ambient air conditions but also in vacuum. Our bioinspired patterned adhesive with an area of 1 cm^2 provided an adhesion force of 2.6 N ± 0.2 N in air, which was reduced to 1.9 N ± 0.2 N if measured in vacuum. Detachment was induced by buckling of the structures due to a high compressive preload and occurred, independent of air pressure, at approximately 0.9 N ± 0.1 N. The switch in adhesion was observed at a compressive preload between 5.6 and 6.0 N and was independent of air pressure. The difference between maximum adhesion force and adhesion force after buckling gives a reasonable window of operation for pick and place processes. High reversibility of the switching behavior is shown over 50 cycles in air and in vacuum, making the bioinspired switchable adhesive applicable for handling operations of fragile objects.

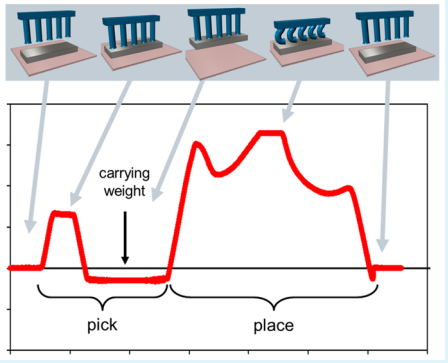

KEYWORDS: *gecko, responsive, switchable, dry adhesive, reversible, vacuum*

1. INTRODUCTION

Animals like flies,[1] ants,[2] or beetles[3] have developed versatile attachment systems which enable them to attach quickly and reversibly to surfaces of varying chemistry and topography, i.e., smooth and rough surfaces. Their contact elements are covered with millions of fine fibrils, which, often in combination with secretions,[4] play a crucial role in adhesion.[5] One of the most complex and efficient adhesion systems is found in geckos, the largest known animals with hairy attachment pads.[6,7] Their attachment system is a "dry" system and does not rely on adhesion enhancing secretions. Although some phospholipids were found in gecko footprints,[8] the function of these lipids seem to be irrelevant for adhesion. The adhesive interaction of gecko toe pads with a surface is mainly based on van der Waals forces,[7] likely enhanced by capillary forces due to humidity.[9,10] Geckos can generate large forces, reaching a surprisingly high shear strength of up to 100 kPa.[6] This performance is assumed to be related to good adaptability of the hairy attachment pads to roughness, an improved stress distribution, an increased defect tolerance, and size effects.[11] Besides the outstanding adhesive properties, a quick and easy release of the adhesive pads is crucial for locomotion and, ultimately, the survival of the gecko. Detachment is controlled by the anisotropy of the adhesive structures and the biomechanics of the gecko's motion, which consists of simultaneous shear and peel movement.[12]

The first systematic investigations of the adhesive mechanisms and the interactions of gecko toe pads with a broad variety of substrates were made in the early 20th century. Weitlaner performed adhesion experiments with living and dead geckos to understand whether the gecko uses a "pneumatic mechanism" for attachment. Despite his very limited experimental equipment, he found that amputated and shear loaded gecko feet did not lose their sticking capability to various surfaces even at reduced air pressure. He concluded that the, at that time assumed, "pneumatic mechanism" does not have an essential impact on the extraordinary adhesive properties of the gecko toe pad but may only have a minor contribution to adhesion.[13] In summary, the gecko's adhesion system combines the following properties: high adhesive forces, quick and easy detachment, dry "residue-free" contact, and operational in vacuum.

Hence, it is not surprising that this attachment system gains growing attention, not only from the scientific community but also from industry, especially as its properties may lead to new artificial attachment devices, which could replace current state of the art systems such as suction cups. Consequently, artificial bioinspired adhesive systems have been extensively studied,[11,14−17] and comparably high adhesive performance was

Received: August 7, 2015
Accepted: October 12, 2015
Published: October 12, 2015

DOI: 10.1021/acsami.5b07287
ACS Appl. Mater. Interfaces 2015, 7, 24127−24135

reached, even exceeding the so-called "gecko-limit" of 100 kPa.[18] In extension to Weitlaner's results on the adhesion of geckos, recent studies suggest that adhesion of (synthetic) bioinspired surfaces relies, in addition to van der Waals interactions, to a small part on suction.[19] It was found experimentally that a small suction effect is present for mushroom-shaped patterned adhesives if adhesion is tested in vacuum.[19−21] It has also been predicted theoretically that suction effects may become relevant in patterned surfaces as soon as a certain critical contact size is exceeded.[22,23]

Many of these bioinspired systems have been applied to grip and release objects; most approaches function close to the directional, shear induced adhesion found for geckos.[12] There, switching adhesion mainly relies on asymmetric adhesive structures, which exhibit high adhesion if sheared into one direction, while adhesion drops significantly if sheared in the opposite direction.[24] The frequently occurring lateral displacement of the object during attachment and detachment may be circumvented by gripper designs, where two or more anisotropic adhesive pads are sheared in opposite directions so that the lateral forces cancel out.[25] Other approaches combine electrostatic adhesion and bioinspired adhesives to maintain a compressive preload on the adhesive structures[26] or even use biological structures obtained from gecko toes for handling of small objects.[27] An approach to handle objects with a more complex geometry is based on a balloon-like gecko adhesive tape, which can be adapted to curved surface geometries by "inflating" and "deflating" the balloon.[28]

Besides fabrication and characterization of bioinspired adhesives with high and robust adhesion and adhesion control using "passive" peeling or shearing, the control of adhesion by an external stimulus[29−33] has been studied and improved to obtain switchable adhesives even in extreme environments like outer space.[34] While the complex detachment motion works efficiently for geckos and has already been mimicked relatively close to the natural archetype,[35] other approaches have emerged to switch adhesion by using external triggers. Shape memory materials,[36,37] active polymeric materials such as liquid crystal elastomers,[38] injection of liquids in subsurface microchannels,[29] application of magnetic fields to orient magnetic structures,[39] or mechanical loading of rubber elastic patterned samples was applied to obtain switchability.[40] The latter has been investigated in detail and shows detachment of rubber elastic pillars due to mechanical instability at high compressive load, leading to a preload responsive switchable adhesive.[40−43] Due to the simplicity of the operation mode and the fast and reversible response, this approach shows significant potential for pick and place processes. In a more recent publication, this approach of pressure activated switchable adhesion was extended by using structures of different length to switch between three adhesive states, namely, low, high, and very low adhesion.[44]

To obtain pick and place handling in vacuum conditions, robust adhesion in vacuum and reliable switchability need to be linked. In the present study, the adhesive performance of a preload responsive, bioinspired adhesive was tested both in vacuum and in air, and the influence of air pressure on adhesion was quantified. Further, pick and place processes were performed and the reversibility was demonstrated over 50 loading cycles.

2. EXPERIMENTAL SECTION

2.1. Mold Preparation. Aluminum molds were fabricated using a process similar to the one reported in earlier studies.[45,46] An array of holes with 2 mm depth, 0.4 mm width, and a center−center spacing of 0.8 mm was milled. The geometrical parameters were chosen to yield samples which possess a mechanical instability at high compressive loading, known to lead to detachment.[40,42] The array contained 203 holes and covered an area of approximately 1 cm^2. The mold was thoroughly cleaned in acetone, ethanol, isopropanol, and deionized water in an ultrasonic bath and subsequently silanized. For this, the mold was placed together with a glass vial containing 10 μL of trichloroperfluorooctysilane (Sigma-Aldrich) into a desiccator and evacuated to a pressure below 10 mbar for at least 45 min until the silane evaporated completely. Afterward, the mold was kept in an oven in air at 95 °C for 2 h.

2.2. Sample Preparation. Samples were prepared from polydimethylsiloxane (PDMS, Sylgard 184, Dow Corning) by soft molding of the previously prepared aluminum molds. The PDMS prepolymer and cross-linker were mixed in a 10:1 ratio, poured onto the silanized mold, and degassed in a desiccator. The filled mold was then placed in an oven and cured at 75 °C for 4 h. After cooling to room temperature, the PDMS sample was carefully peeled from the mold, resulting in a PDMS array of cylindrical pillars. The backing layer was approximately 3 mm thick.

2.3. Tip Modification. Pillars with mushroom-shaped tips were reported to significantly increase adhesion compared to pillars having flat or spherical tips.[18,45,47] Thus, the tips were modified using a variation of a previously described process.[18] Briefly, PDMS was mixed and degassed as described above. A thin metal rod was dipped into the liquid PDMS and gently brought into contact with the pillars, resulting in deposition of a small droplet of liquid PDMS on the tip of each pillar. Afterward, the droplet-covered tips were placed face-down onto a smooth, silanized glass plate (silanization protocol as above). The tips were squashed, resulting in a flattened mushroom-shape. The patterned sample was fully cured in an oven at 75 °C for 4 h and, after cooling to room temperature, carefully removed from the glass plate. Three samples were chosen for adhesion experiments; an exemplary sample is shown in Figure 1a.

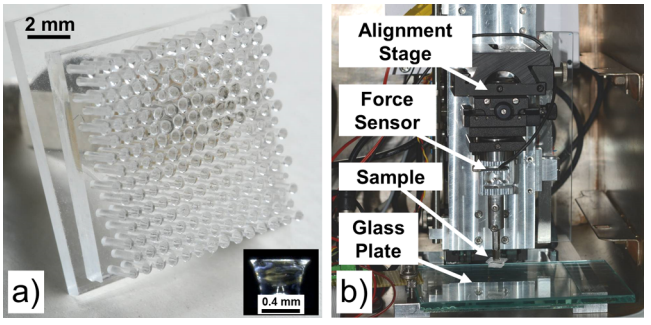

Figure 1. (a) The photograph shows an exemplary bioinspired switchable dry adhesive PDMS sample with an array of mushroom-shaped pillars. The inset exhibits a side view of a single mushroom shaped tip. (b) The experimental adhesion tester setup is built in a vacuum oven for experiments at ambient air pressure and at low pressure condition (<10 mbar).

2.4. Adhesion Testing Setup. An adhesion measurement setup as shown in Figure 1b, inspired by the macroscopic adhesion measurement device (MAD),[48] was built in a vacuum oven. It consisted of a linear z-positioning system and a load-cell based force measurement. Each patterned PDMS sample was fixated to a glass backing by applying oxygen plasma to the backside of the sample and bringing it into contact with the smooth cleaned glass plate. The sample was mounted to a load cell with a stiffness of >100 kN/m. Prior to the adhesion measurements, the sample was aligned using a manual alignment stage and applying the alignment process published

DOI: 10.1021/acsami.5b07287
ACS Appl. Mater. Interfaces 2015, 7, 24127−24135

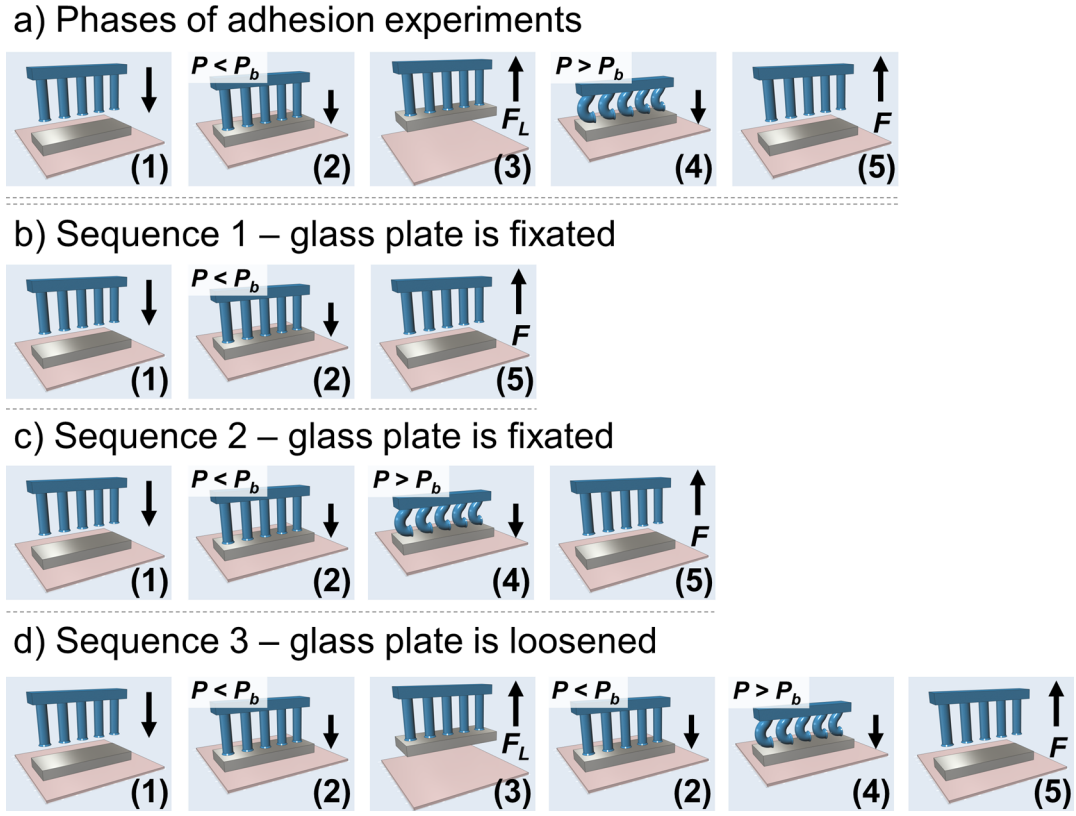

Figure 2. (a) Schematic of different phases during adhesion experiments; (1) the sample with the rubber elastic pillars is moved toward the glass slide, (2) attachment occurs and a preload $P < P_b$ is applied, (3) the sample is moved upward, lifting the glass plate with the lifting force F_L, (4) a preload $P > P_b$ is applied, where buckling of the pillars occurs, and (5) pull-off from the glass plate with the force F. The different sequences are schematically given in (b, c, and d).

by Kroner et al.[49] Force and displacement were recorded during all measurements.

2.5. Adhesion Measurements. All experiments were performed with a testing velocity of 80 μm/s. Each sample was tested at least three times and thereby rotated by ~120° along the vertical axis in between the experiments to avoid misalignment. Adhesion measurements were conducted in ambient atmosphere, called "air" in the subsequent text, and at reduced pressure <10 mbar, called "vacuum" in the subsequent text. A glass plate was used as test substrate which was, depending on the testing mode, either fixated or loosened. To obtain an equilibrium surface state, more than 300 contacts were made between a smooth PDMS sample and the glass plate prior to adhesion measurements.[50,51] The experimental error for all adhesion measurements was ±0.1 N.

Different phases occurred during an adhesion experiment with preload responsive dry-adhesive samples, which are schematically shown in Figure 2a and can be described as follows:

- Phase (1): The aligned sample is moved toward the smooth glass plate.
- Phase (2): The sample forms contact with the glass plate, and a compressive preload P below the critical buckling preload P_b is applied.[40] The load is kept for at least three seconds.
- Phase (3): The sample is retracted and, due to adhesion, the glass plate is lifted with a force F_L. This phase only applies if the glass plate is loosened.
- Phase (4): A preload above the critical buckling preload P_b is applied, causing the structures to buckle and the structure tips to detach from the glass probe.[40]
- Phase (5): The sample is retracted from the glass plate, and the pull-off force F, defined as the absolute value of the maximum negative force of the recorded force–time curves, is measured.

These phases can be grouped into different sequences to represent specific adhesion measurements. The following sequences were applied:

- Sequence 1 (Figure 2b): The preload P is chosen so that contact is formed with the glass plate, but no buckling of the structures occurs.[40] The glass plate is fixated to prevent it from lifting. This experiment corresponds to the phases (1) (2) (5).
- Sequence 2 (Figure 2c): In this sequence, a preload P above the critical buckling load P_b is applied.[40] The glass plate is also fixated. This experiment is represented by the phases (1) (2) (4) (5).
- Sequence 3 (Figure 2d): A pick and place process is imitated using a loosened glass plate. A preload P below the buckling load P_b is applied and the glass plate is lifted, which corresponds to the phases (1) (2) (3). In the next step, the glass plate is lowered and detached using a preload P above the buckling load P_b, which corresponds to the phases (2) (4) (5). The complete pick and place process is described by phases (1) (2) (3) (2) (4) (5).

2.6. Applied Measurement Sets. To determine the adhesive properties of the switchable bioinspired adhesive and its applicability for pick and place processes, the following measurement sets and analyses were conducted in air and vacuum conditions:

(i) Force–time curves were recorded for different preloads up to 7 N, allowing determination of the preload dependent pull-off force behavior of the switchable adhesive. The pull-off force F (absolute value of the maximum detachment force) was plotted as a function of preload P, leading to the identification of the buckling preload P_b.[40] These measurements correspond to sequence 1 for $P < P_b$ and sequence 2 for $P > P_b$.

(ii) Exemplary force–time curves from (i) were analyzed for two selected measurements, one having a preload $P < P_b$ according

DOI: 10.1021/acsami.5b07287
ACS Appl. Mater. Interfaces 2015, 7, 24127–24135

to sequence 1, and one having a preload $P > P_b$ according to sequence 2.

(iii) Adhesion experiments with sequence 1 directly followed by sequence 2 were repeated 50 times to test for reversibility.

(iv) Force–time curves were recorded for a pick and place process represented by sequence 3. The glass plate with a weight of 65 g was lifted for at least 10 s during phase (3). Reversibility was again tested by repeating this sequence for 50 times.

3. RESULTS

The experimental results of the different measurement sets are described in the following four subsections.

3.1. Measurement Set (i): Preload Dependent Pull-off Force. Pull-off forces F were measured as a function of preload and are given in Figure 3. The pull-off force was found to be almost preload independent at low preloads. As soon as a critical preload was applied, the pull-off force dropped significantly which corresponded to the optically observed elastic buckling of the pillars. The critical buckling preload P_b was highly reproducible for each sample but showed some variation in a range from 5.6 to 6.0 N for different samples. For preloads $P < P_b$, the pull-off forces were between 2.5 and 2.7 N in air, while experiments in vacuum resulted in pull-off forces between 1.8 and 1.9 N. It can be clearly seen that, for lower preloads, the pull-off force depends on the air pressure; adhesion was reduced by about 30% in vacuum. For $P > P_b$, the pull-off force was found to be 0.9 N and was independent of air pressure.

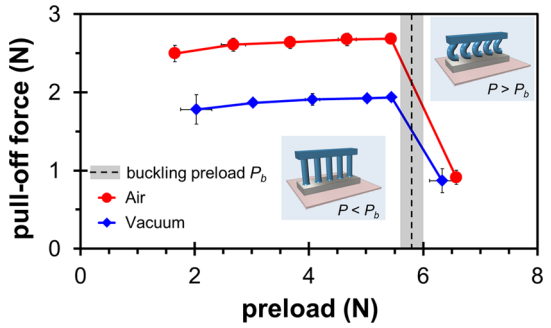

Figure 3. Absolute values of the pull-off forces are plotted as a function of applied preload, measured in air and in vacuum. At a critical preload P_b, indicated by the dashed line within the gray area, buckling of the pillars was observed.

3.2. Measurement Set (ii): Force–Time Curves. Exemplary force–time curves with preload $P < P_b$ and $P > P_b$, respectively, measured in air and vacuum, are plotted in Figure 4.

Figure 4a,b depicts exemplary force–time curves of adhesion measurements with a preload $P < P_b$, which corresponds to sequence 1. The sample was moved toward the fixated glass plate, formed contact, and was loaded, until the preload P was reached. In these examples, the preload P was 3.7 N for testing in air (Figure 4a) and 4.0 N for testing in vacuum (Figure 4b). The load was applied for at least 3 s. Then, the sample was retracted again, leading to an adhesive (tensile) force, ultimately reaching the maximum pull-off force F. The negative sign indicates the direction of force measurement. For these measurements, a pull-off force F of 2.6 N was found in air (Figure 4a) and of 1.9 N (Figure 4b) in vacuum.

Representative force–time curves, where a preload $P > P_b$ was applied corresponding to sequence 2, are shown in Figure 4c,d. The sample was approached, formed contact with the glass probe, and was loaded. The compressive force increased during loading until a local maximum occurred at a critical load P_b of 5.8 N. Subsequently, the compressive force decreased rapidly with ongoing compression and buckling of the pillars was optically observed. As the pillars were bent further with increasing displacement, the compressive force increased again until the predefined preload P was reached and kept for at least 3 s. In Figure 4c, the preload was 6.6 N, and in Figure 4d, the preload was 6.3 N. The reverse force–time behavior was observed during retraction; the occurring maximum corresponded to an optically observed "unbuckling" of the pillars. A pull-off force F of 0.9 N was recorded during retraction, both for measurements in air and in vacuum. These force–time curves for a preload $P > P_b$ are characteristic for the buckling

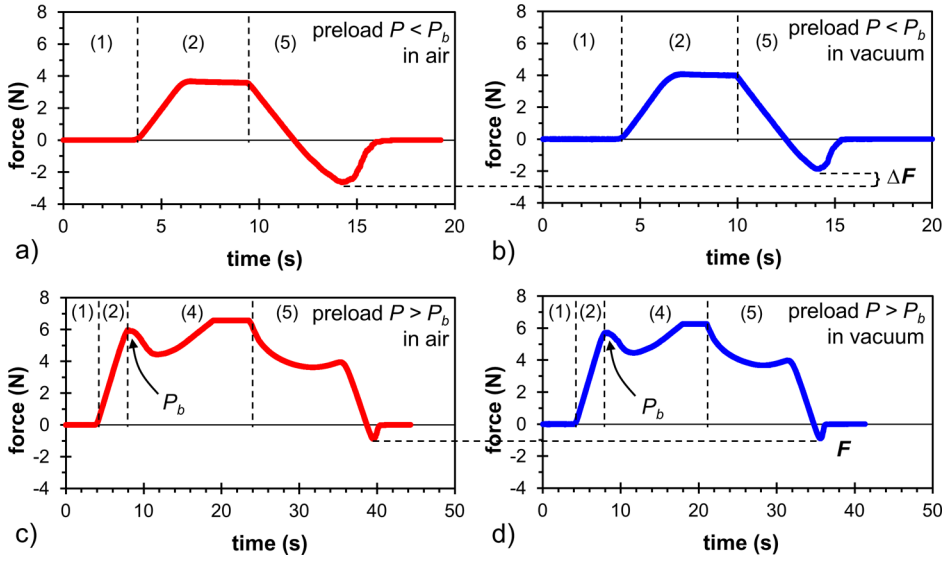

Figure 4. Representative force–time curves for adhesion experiments of bioinspired dry adhesives on a fixated glass plate. Measurements using sequence 1 with a preload P below the buckling preload P_b in (a) air and (b) in vacuum. Measurements using sequence 2 with a preload P above the buckling preload P_b (c) in air and d) in vacuum. The phases from Figure 2a are indicated.

DOI: 10.1021/acsami.5b07287
ACS Appl. Mater. Interfaces 2015, 7, 24127–24135

behavior and have been reported and characterized in earlier studies.[40]

The force−time curves are very similar for experiments in air and in vacuum. A significant difference was found only in the pull-off force F; experiments with a preload $P < P_b$ resulted in a change in pull-off force F from 2.6 to 1.9 N, which is equal to a loss in adhesion of approximately 30%. For a preload $P > P_b$, the pull-off force F was substantially lower, reaching only 0.9 N, and did not differ between air and vacuum condition.

3.3. Measurement Set (iii): Reversibility. To evaluate the reversibility of the switching behavior between high and low pull-off force, alternating preloads below and above P_b were applied. 50 cycles of the sequence 1, directly followed by sequence 2, were performed in air and in vacuum according to the measurement set (iii). Figure 5 shows the recorded forces,

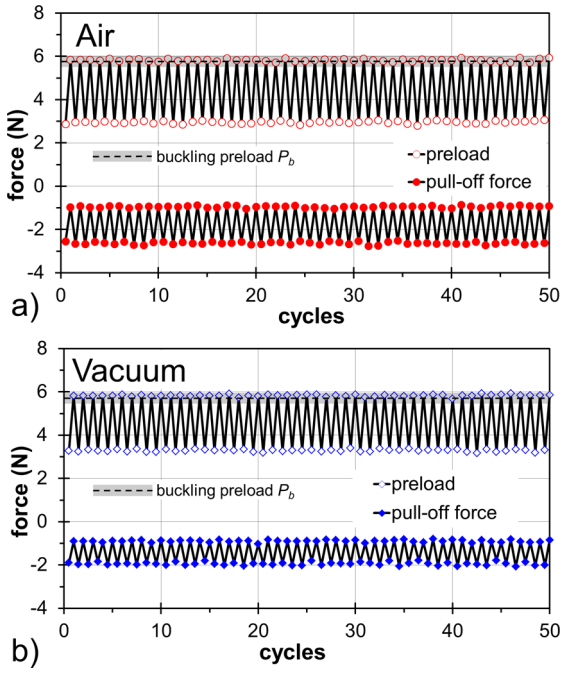

Figure 5. Reversibility tests of adhesion measurements with alternating preload below and above the buckling load, described by sequence 1, directly followed by sequence 2. Each plot shows the applied preload P and the resulting pull-off force F over 50 test cycles (a) in air and (b) in vacuum. Note that the pull-off force F is not given as absolute value here but has a negative sign for clarity of the diagram.

namely, the preload P and the pull-off force F, as a function of testing cycles. Note that the pull-off force F is not given as absolute value but has a negative sign for clarity of the diagram. In air (Figure 5a), the alternating preloads P of 2.9 and 5.8 N resulted in adhesive forces F of 2.6 and 0.9 N, respectively. In vacuum (Figure 5b), the applied preloads P were 3.3 and 5.8 N, which resulted in adhesive forces F of 1.9 and 0.9 N, respectively. No notable changes in pull-off force were found within the 50 test cycles.

3.4. Measurement Set (iv): Pick and Place. A pick and place process, corresponding to the sequence 3 in Figure 2d, was simulated. As described in the measurement set (iv), an alternating preload below and above the buckling load P_b was applied with the glass plate being loosened to allow lifting. Representative force−time curves in air and in vacuum are given in Figure 6a,b, respectively. The graphs show no notable differences, indicating that the lifting process and the release of

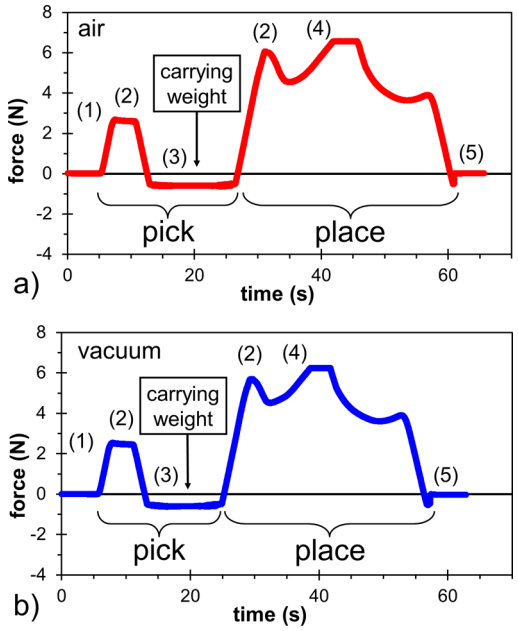

Figure 6. Force−time curves of a pick and place process, where a glass plate of 65 g is lifted and released again. The experiment corresponds to the sequence 3; the numbers indicate the respective phases from Figure 2. The measurements were performed (a) in air and (b) in vacuum.

the glass plate were comparable in both air and vacuum conditions. An exemplary video of a pick and place process is shown in the Supporting Information, using a silicon wafer instead of a glass plate for the sake of better visibility.

4. DISCUSSION

On the basis of the experimental results, the following properties of the pressure actuated adhesive system in air and vacuum conditions were analyzed: the adhesive properties, the reversibility of switching, and the adaptability for pick and place processes.

The adhesive properties, represented by the force−time curves, are given in Figure 4. The curves exhibit a characteristic shape which is typical for patterned bioinspired adhesives such as the tested samples. Low preload leads to a comparably high pull-off force, while high preload results in buckling of the structures at a certain buckling preload P_b, which reduces adhesion significantly.[40] The mechanism of adhesion loss has been investigated in an earlier study, where it was found that the unbuckling during unloading does not allow reformation of intimate contact between the pillar tips and the probe.[40] The lack of intimate contact between pillar tips and probe causes a reduction in adhesion. The adhesive behavior in air and vacuum conditions is qualitatively similar, indicating that the mechanism of adhesion loss by buckling is unaffected by air pressure. The main influence of air pressure on the adhesive properties is found in the magnitude of the pull-off force, which can be seen in Figures 3 and 4a,b (indicated as ΔF). The pull-off force F was found to be between 2.5 and 2.7 N in air and 1.8 and 1.9 N in vacuum, respectively, exhibiting that the application of vacuum reduces adhesion by ΔF of 0.7 N ± 0.2 N, which corresponds to a loss in adhesion of approximately 30%. This reduction becomes obvious by considering Figure 3; all pull-off forces obtained in vacuum lie below the ones obtained in air if

DOI: 10.1021/acsami.5b07287
ACS Appl. Mater. Interfaces 2015, 7, 24127−24135

the preload was chosen to be below the critical buckling preload P_b.

We identified two factors which may be responsible for the varying adhesion with changing air pressure, namely, humidity and suction. We tend to exclude humidity and favor suction as the main mechanism for the change in pull-off force for the following reasons. PDMS is a hydrophobic material which does not tend to absorb water in larger quantities. In addition, it was found that no measurable humidity effect is present at humidity between 2% and 90% for smooth PDMS surfaces and for pillar arrays with diameters of 25 μm.[9] Huber et al. found an additional adhesion effect in the presence of humidity and explained it by a smoothening effect of the water on rough surfaces,[52] but the tested surfaces in this study are expected to be smooth. These points indicate that capillarity effects may have a minor influence on the adhesion in our experiments.

In contrast, suction effects on mushroom shaped pillars are expected from theoretical considerations[23] and were also found in earlier experimental studies.[19,20] It was shown that suction is present for adhesive pillars with mushroom-shaped tips and can contribute considerably to adhesion with up to 10% of the pull-off force.[19] In our case, the suction component even exceeds this percentage, reaching approximately 30%. While adhesion experiments in air result in pull-off forces between 2.5 and 2.7 N, the same set of experiments in vacuum exhibits pull-off forces between 1.8 and 1.9 N. This difference may be explained by the size of the pillars. Suction based forces scale with the area of the contact, while adhesion of patterned surfaces due to van der Waals forces was theoretically and experimentally shown to scale with length.[53,54]

Theoretically, the suction force $F_{suction}$ of a perfect suction cup, disregarding other adhesive interactions than suction, is given by the contact area $A_{contact}$ and the pressure difference ΔP caused by the suction effect:

$$F_{suction} = \Delta P \times A_{contact} \quad (1)$$

Consequently, the pull-off strength of a perfect suction cup is directly proportional to the pressure difference inside the contact area and outside the suction cup. For ideal vacuum (0 bar) and atmospheric pressure (~1 bar), a suction force of ~10 N/cm^2 can be achieved using eq 1. Such high values are usually not obtained using typical suction cups.

To compare our experimentally derived pull-off strength values to the performance of typical suction cups, we have converted given data from commercial macroscopic silicone suction cups.[55] The performance of the analyzed suction cups with diameters between 2.6 and 51.4 mm lie between 2.8 and 7.3 N/cm^2 if a compressive stress of 9.0 N/cm^2 is applied;[55] see also Table 1. For comparing these pull-off strength data with our results, it is important to consider that the strength data from the present study reflects the apparent contact strength. Thus, reduction in "real" contact area due to the pillar packing density of ~30% has to be taken into account. A comparable pull-off performance between conventional suction cups and the experiments from our studies would then result in a corrected strength, which is calculated by multiplying the given pull-off strength of the commercial suction cups with the pillar packing density of ~30% from our samples. These values are also given in Table 1.

As can be seen from the corrected pull-off strengths, values between 0.9 and 2.2 N/cm^2 can be considered as typical for commercial suction cups. Our experimentally derived suction component to the pull-off force lies slightly below the lowest suction force of 0.85 N. As the mushroom shaped structures in our study were not specifically optimized for suction, these results fit astonishingly well to the values provided for commercial suction cups.

Table 1. Geometric Parameters of Commercial Suction Cups and Their Adhesive Performance after Attaching Them with a Compressive Load of 9.0 N/cm^2 [a]

diameter, mm	contact area, mm^2	force, N	strength, N/cm^2	corrected strength, N/cm^2
2.6	5.3	0.15	2.8	0.9
3.8	11.3	0.65	5.7	1.7
5.0	19.6	1.3	6.6	2.0
7.0	38.5	2.5	6.5	2.0
9.0	63.6	3.9	6.1	1.8
11.0	95.0	6.9	7.3	2.2
16.5	213.8	11.0	5.1	1.5
22.0	380.1	16.0	4.2	1.3
32.0	804.2	30.0	3.7	1.1
41.0	1320.3	49.0	3.7	1.1
51.4	2075.0	92.0	4.4	1.3

[a]The corrected strength assumes a packing density of 30%, data after ref 55.

It was reported that suction and van der Waals interactions have a different size effect.[23] Thus, we expect that the suction effect becomes more prominent with increasing size of the contact elements, while reducing the size of the contact elements diminishes the influence of suction.

Consequently, if suction caused the change in adhesion of the present experiments, it would be strongly influenced by the contact geometry. During the buckling process, the mushroom tips detach and the pillars form side contact with the glass plate. This contact geometry does not allow building up a difference in air pressure, thereby diminishing the suction component of the pull-off force. Our experiments show that the application of a load exceeding P_b leads to a pull-off force F of 0.9 N, both in air and in vacuum. This phenomenon is also reflected in Figure 3; while the pull-off forces at a preload below P_b differ for measurements in air and in vacuum, similar pull-off forces are found if the buckling preload P_b is overcome. These observations support the assumption that air pressure enhances adhesion due to suction in patterned bioinspired surfaces with structure sizes in the macroscopic range, while detachment events after buckling of the pillars are not affected by air pressure, since suction cannot be maintained after buckling has occurred. This leads to the conclusion that the difference in pull-off force of the bioinspired adhesive is not a result of changing humidity but is caused most likely by a suction effect.

For a better description of the switching behavior, a switching efficiency S is introduced in eq 2, which is defined by the ratio of the pull-off forces at a preload above and below the buckling preload P_b:

$$S = 1 - \frac{F(P > P_b)}{F(P < P_b)} \quad (2)$$

.

A value of $S = 0$ indicates no switching behavior, and $S = 1$ resembles a perfect switch where adhesion can be completely turned on and off. If eq 2 is applied to the obtained experimental data, the switching efficiency S is approximately 0.65 ± 0.07 in air, while a value of $S = 0.50 \pm 0.1$ is obtained in vacuum. Thus, applying vacuum reduces the switching

DOI: 10.1021/acsami.5b07287
ACS Appl. Mater. Interfaces 2015, 7, 24127−24135

efficiency by a mean value of $\Delta S = 0.15$. These calculated efficiencies indicate that the switch in adhesion may be further improved. Still, the reached values allow a significant change in adhesion in air and in vacuum, opening a sufficiently large window of operation for pick and place applications.

These promising results are promoted by the reversibility test shown in Figure 5, which indicates that the switch in adhesion is highly reversible in air and in vacuum. No change in adhesive performance or damage of the dry adhesive structures was detected after 50 testing cycles. Finally, pick and place processes were conducted using a glass plate with a weight of 65 g. The glass plate was securely lifted and released in air and in vacuum. No significant difference is observed in the adhesion curves given in Figure 6 for operation at both air pressure conditions. Hence, the pick and place process is not notably influenced by the reduction of air pressure.

It should be mentioned that the pick and release process has two restrictions for operation if a reliable switch in adhesion is required. First, if the object to be lifted is too light, the pull-off force after application of a preload above the buckling preload P_b may be too high for reliable detachment, representing a minimum weight threshold, and second, if the object to be lifted is too heavy, it will detach prior to lifting, representing a maximum weight threshold. It follows that an optimum range of operation can be defined on the basis of the pull-off forces measured for a preload below, and above, the buckling preload P_b. For the tested samples, the range of operation can be determined to be between approximately 0.9 and 2.5 N in air or between 0.9 and 1.8 N in vacuum. It further has to be considered that the viscoelasticity of the applied material may have a significant influence in the buckling of the structures and may shift both the lower and the higher boundary of the range of operation. This window of operation may be tuned according to the envisaged application, for example, by changing the number of pillars, by their packing density, by further modification of their tip geometry, or by a different choice of sample material.

5. CONCLUSIONS

The present study showed that bioinspired switchable adhesion based on reversible buckling of elastic pillars is applicable in vacuum. At low compressive load, the pull-off force for samples with sizes of 1 cm^2 was between 2.5 and 2.7 N (±0.1 N) in air and was reduced to 1.8 to 1.9 N (±0.1 N) if measured in vacuum. This indicates that a suction component was present in the attachment state, since an influence of humidity may be excluded. Application of a compressive load above the buckling preload P_b between 5.6 and 6.0 N (±0.1 N) caused a reversible buckling of the pillars and resulted in pull-off forces of 0.9 N (±0.1 N), which were similar for experiments in air and in vacuum. This indicates the absence of a suction component after buckling of the pillars occurred. Our experiments exhibited that the transition between the two adhesive states was sharp and the switching behavior was independent of air pressure. Further, the switch in adhesion exhibited high reversibility; we showed that the system works reliably in air and in vacuum for 50 pick and place cycles without any signs of wear or change in adhesion performance. The functionality of the switchable adhesive at low air pressure makes it applicable for handling operations of fragile objects in vacuum.

ASSOCIATED CONTENT

Supporting Information

The Supporting Information is available free of charge on the ACS Publications website at DOI: 10.1021/acsami.5b07287.

Video showing an exemplary pick and place process using a switchable bioinspired adhesive to handle a silicon wafer (AVI)

AUTHOR INFORMATION

Corresponding Author

*E-mail: elmar.kroner@leibniz-inm.de. Phone: +49 (0) 681 9300 369.

Author Contributions

§J.P., M.F., and E.K. contributed equally.

Funding

The research leading to these results was conducted within a Grant of the European Research Council under the European Union's Seventh Framework Program (FP/2007-2013)/ERC Grant Agreement No. 340929, awarded to E. Arzt.

Notes

The authors declare no competing financial interest.

ACKNOWLEDGMENTS

The authors thank the Mechanical Workshop of the INM for mold fabrication, Susanne Selzer and Ina Kothe for their help in sample preparation, and Joachim Blau for building up the adhesion measurement setup.

ABBREVIATIONS

CVD = chemical vapor deposition
PVD = physical vapor deposition
PDMS = polydimethylsiloxane
MAD = macroscopic adhesion measurement device

REFERENCES

(1) Langer, M. G.; Ruppersberg, J. P.; Gorb, S. Adhesion Forces Measured at the Level of a Terminal Plate of the Fly's Seta. *Proc. R. Soc. London, Ser. B* **2004**, *271* (1554), 2209−2215.
(2) Federle, W.; Rohrseitz, K.; Holldobler, B. Attachment Forces of Ants Measured with a Centrifuge: Better "Wax-Runners" have a Poorer Attachment to a Smooth Surface. *J. Exp. Biol.* **2000**, *203* (3), 505−512.
(3) Stork, N. E. Experimental Analysis of Adhesion of Chrysolina Polita (Chrysomelidae: Coleoptera) on a Variety of Surfaces. *J. Exp. Biol.* **1980**, *88* (1), 91−108.
(4) Federle, W. Why Are So Many Adhesive Pads Hairy? *J. Exp. Biol.* **2006**, *209*, 2611−2621.
(5) Jagota, A.; Bennison, S. J. Mechanics of Adhesion Through a Fibrillar Microstructure. *Integr. Comp. Biol.* **2002**, *42* (6), 1140−1145.
(6) Autumn, K.; Liang, Y. A.; Hsieh, S. T.; Zesch, W.; Chan, W. P.; Kenny, T. W.; Fearing, R.; Full, R. J. Adhesive Force of a Single Gecko Foot-Hair. *Nature* **2000**, *405* (6787), 681−685.
(7) Autumn, K.; Sitti, M.; Liang, Y. A.; Peattie, A. M.; Hansen, W. R.; Sponberg, S.; Kenny, T. W.; Fearing, R.; Israelachvili, J. N.; Full, R. J. Evidence for Van Der Waals Adhesion in Gecko Setae. *Proc. Natl. Acad. Sci. U. S. A.* **2002**, *99* (19), 12252−12256.
(8) Hsu, P. Y.; Ge, L.; Li, X.; Stark, A. Y.; Wesdemiotis, C.; Niewiarowski, P. H.; Dhinojwala, A. Direct Evidence of Phospholipids in Gecko Footprints and Spatula−Substrate Contact Interface Detected using Surface-Sensitive Spectroscopy. *J. R. Soc., Interface* **2012**, *9* (69), 657−664.
(9) Buhl, S.; Greiner, C.; del Campo, A.; Arzt, E. Humidity Influence on the Adhesion of Biomimetic Fibrillar Surfaces. *Int. J. Mater. Res.* **2009**, *100* (8), 1119−1126.

DOI: 10.1021/acsami.5b07287
ACS Appl. Mater. Interfaces 2015, 7, 24127−24135

(10) Huber, G.; Gorb, S. N.; Hosoda, N.; Spolenak, R.; Arzt, E. Influence of Surface Roughness on Gecko Adhesion. *Acta Biomater.* **2007**, *3* (4), 607−610.
(11) Kamperman, M.; Kroner, E.; del Campo, A.; McMeeking, R. M.; Arzt, E. Functional Adhesive Surfaces with "Gecko" Effect: The Concept of Contact Splitting. *Adv. Eng. Mater.* **2010**, *12* (5), 335−348.
(12) Autumn, K.; Dittmore, A.; Santos, D.; Spenko, M.; Cutkosky, M. Frictional Adhesion: a New Angle on Gecko Attachment. *J. Exp. Biol.* **2006**, *209* (18), 3569−3579.
(13) Kroner, E.; Davis, C. S. A Study of the Adhesive Foot of the Gecko Translation of a Publication of Dr. F. Weitlaner. *J. Adhes.* **2015**, *91* (6), 481−487.
(14) Heepe, L.; Gorb, S. Biologically Inspired Mushroom-Shaped Adhesive Microstructures. *Annu. Rev. Mater. Res.* **2014**, *44*, 173−203.
(15) Pattantyus-Abraham, A.; Krahn, J.; Menon, C. Recent Advances in Nanostructured Biomimetic Dry Adhesives. *Front. Bioeng. Biotechnol.* **2013**, *1* (22); DOI: 10.3389/fbioe.2013.00022
(16) Sameoto, D.; Menon, C. Recent Advances in the Fabrication and Adhesion Testing of Biomimetic Dry Adhesives. *Smart Mater. Struct.* **2010**, *19* (10), 103001.
(17) Zhou, M.; Pesika, N.; Zeng, H.; Tian, Y.; Israelachvili, J. Recent Advances in Gecko Adhesion and Friction Mechanisms and Development of Gecko-Inspired Dry Adhesive Surfaces. *Friction* **2013**, *1* (2), 114−129.
(18) Del Campo, A.; Greiner, C.; Arzt, E. Contact Shape Controls Adhesion of Bioinspired Fibrillar Surfaces. *Langmuir* **2007**, *23* (20), 10235−10243.
(19) Heepe, L.; Varenberg, M.; Itovich, Y.; Gorb, S. N. Suction Component in Adhesion of Mushroom-Shaped Microstructure. *J. R. Soc., Interface* **2011**, *8* (57), 585−589.
(20) Davies, J.; Haq, S.; Hawke, T.; Sargent, J. P. A Practical Approach to the Development of a Synthetic Gecko Tape. *Int. J. Adhes. Adhes.* **2009**, *29* (4), 380−390.
(21) Sameoto, D.; Sharif, H.; Menon, C. Investigation of Low-Pressure Adhesion Performance of Mushroom Shaped Biomimetic Dry Adhesives. *J. Adhes. Sci. Technol.* **2012**, *26* (23), 2641−2652.
(22) Afferrante, L.; Carbone, G. The Mechanisms of Detachment of Mushroom-Shaped Micro-Pillars: From Defect Propagation to Membrane Peeling. *Macromol. React. Eng.* **2013**, *7* (11), 609−615.
(23) Spolenak, R.; Gorb, S.; Gao, H.; Arzt, E. Effects of Contact Shape on the Scaling of Biological Attachments. *Proc. R. Soc. London, Ser. A* **2005**, *461* (2054), 305−319.
(24) Mengüç, Y.; Yang, S. Y.; Kim, S.; Rogers, J. A.; Sitti, M. Gecko-Inspired Controllabe Adhesive Structures Appied to Micromanipulation. *Adv. Funct. Mater.* **2012**, *22* (6), 1246−1254.
(25) Zhou, M.; Tian, Y.; Sameoto, D.; Zhang, X.; Meng, Y.; Wen, S. Controllable Interfacial Adhesion Applied to Transfer Light and Fragile Objects by Using Gecko Inspired Mushroom-Shaped Pillar Surface. *ACS Appl. Mater. Interfaces* **2013**, *5*, 10137−10144.
(26) Ruffatto, D.; Parness, A.; Spenko, M. Improving Controllable Adhesion on Both Rough and Smooth Surfaces with a Hybrid Electrostatic/Gecko-Like Adhesive. *J. R. Soc., Interface* **2014**, *11* (93), 20131089.
(27) Jeong, J.; Kim, J.; Song, K.; Autumn, K.; Lee, J. Geckopringint: Assembly of Microelectronic Devices on Unconventional Surfaces by Transfer Printing with Isolated Gecko Setal Arrays. *J. R. Soc., Interface* **2014**, *11* (99), 20140627.
(28) Song, S.; Sitti, M. Soft Grippers Using Micro-Fibrillar Adhesives for Transfer Printing. *Adv. Mater.* **2014**, *26* (28), 4901−4906.
(29) Arul, E. P.; Ghatak, A. Control of Adhesion via Internally Pressurized Subsurface Microchannels. *Langmuir* **2012**, *28* (9), 4339−4345.
(30) Kier, W. M.; Smith, A. M. The Structure and Adhesive Mechanism of Octopus Suckers. *Integr. Comp. Biol.* **2002**, *42* (6), 1146−1153.
(31) Jeong, H. E.; Kwak, M. K.; Suh, K. Y. Stretchable, Adhesion-Tunable Dry Adhesive by Surface Wrinkling. *Langmuir* **2010**, *26* (4), 2223−2226.
(32) Kim, S.; Sitti, M.; Xie, T.; Xiao, X. Reversible Dry Micro-Fibrillar Adhesives with Thermally Controllable Adhesion. *Soft Matter* **2009**, *5* (19), 3689−3693.
(33) Nadermann, N.; Ning, J.; Jagota, A.; Hui, C. Y. Active Switching of Adhesion in a Film-Terminated Fibrillar Structure. *Langmuir* **2010**, *26* (19), 15464−15471.
(34) Henrey, M.; Tellez, J. P. D.; Wormnes, K.; Pambaguian, L.; Menon, C. Towards the Use of Mushroom-Capped Dry Adhesives in Outer Space: Effects of Low Pressure and Temperature on Adhesion Strength. *Aerosp. Sci. Technol.* **2013**, *29* (1), 185−190.
(35) Kwak, M. K.; Pang, C.; Jeong, H.-E.; Kim, H.-N.; Yoon, H.; Jung, H.-S.; Suh, K.-Y. Towards the Next Level of Bioinspired Dry Adhesives: New Designs and Applications. *Adv. Funct. Mater.* **2011**, *21* (19), 3606−3616.
(36) Frensemeier, M.; Kaiser, J. S.; Frick, C. P.; Schneider, A. S.; Arzt, E.; Fertig, R. S.; Kroner, E. Temperature-Induced Switchable Adhesion using Nickel−Titanium−Polydimethylsiloxane Hybrid Surfaces. *Adv. Funct. Mater.* **2015**, *25* (20), 3013−3021.
(37) Reddy, S.; Del Campo, A.; Arzt, E. Bioinspired Surfaces with Switchable Adhesion. *Adv. Mater.* **2007**, *19*, 3833−3837.
(38) Cui, J.; Drotlef, D.-M.; Larraza, I.; Fernández-Blázquez, J. P.; Boesel, L. F.; Ohm, C.; Mezger, M.; Zentel, R.; del Campo, A. Bioinspired Actuated Adhesive Patterns of Liquid Crystalline Elastomers. *Adv. Mater.* **2012**, *24* (34), 4601−4604.
(39) Northen, M. T.; Greiner, C.; Arzt, E.; Turner, K. L. A Gecko-Inspired Reversible Adhesive. *Adv. Mater.* **2008**, *20* (20), 3905−3909.
(40) Paretkar, D.; Kamperman, M.; Schneider, A. S.; Martina, D.; Creton, C.; Arzt, E. Bioinspired Pressure Actuated Adhesive System. *Mater. Sci. Eng., C* **2011**, *31* (6), 1152−1159.
(41) Paretkar, D.; Kamperman, M.; Martina, D.; Zhao, J.; Creton, C.; Lindner, A.; Jagota, A.; McMeeking, R.; Arzt, E. Preload-Responsive Adhesion: Effects of Aspect Ratio, Tip Shape and Alignment. *J. R. Soc., Interface* **2013**, *10* (83), 20130171; DOI: 10.1098/rsif.2013.0171
(42) Paretkar, D.; Schneider, A. S.; Kroner, E.; Arzt, E. In Situ Observation of Contact Mechanisms in Bioinspired Adhesives at High Magnification. *MRS Commun.* **2011**, *1* (1), 53−56.
(43) Varenberg, M.; Gorb, S. Close-Up of Mushroom-Shaped Fibrillar Adhesive Microstructure: Contact Element Behaviour. *J. R. Soc., Interface* **2008**, *5* (24), 785−789.
(44) Isla, P. Y.; Kroner, E. A Novel Bioinspired Switchable Adhesive with Three Distinct Adhesive States. *Adv. Funct. Mater.* **2015**, *25* (16), 2444−2450.
(45) Kroner, E.; Arzt, E. Single Macropillars as Model Systems for Tilt Angle Dependent Adhesion Measurements. *Int. J. Adhes. Adhes.* **2012**, *36*, 32−38.
(46) Kroner, E.; Arzt, E. Mechanistic Analysis of Force-Displacement Measurements on Macroscopic Single Adhesive Pillars. *J. Mech. Phys. Solids* **2013**, *61* (6), 1295−1304.
(47) Micciché, M.; Arzt, E.; Kroner, E. Single Macroscopic Pillars as Model System for Bioinspired Adhesives: Influence of Tip Dimension, Aspect Ratio, and Tilt Angle. *ACS Appl. Mater. Interfaces* **2014**, *6* (10), 7076−7083.
(48) Kroner, E.; Blau, J.; Arzt, E. Note: An Adhesion Measurement Setup for Bioinspired Fibrillar Surfaces using Flat Probes. *Rev. Sci. Instrum.* **2012**, *83* (1), 106101.
(49) Kroner, E.; Paretkar, D.; McMeeking, R.; Arzt, E. Adhesion of Flat and Structured PDMS Samples to Spherical and Flat Probes: A Comparative Study. *J. Adhes.* **2011**, *87* (5), 447−465.
(50) Kroner, E.; Maboudian, R.; Arzt, E. Effect of Repeated Contact on Adhesion Measurements Involving Polydimethylsiloxane Structural Material. *IOP Conf. Ser.: Mater. Sci. Eng.* **2009**, *5*, 012004.
(51) Kroner, E.; Maboudian, R.; Arzt, E. Adhesion Characteristics of PDMS Surfaces During Repeated Pull-Off Force Measurements. *Adv. Eng. Mater.* **2010**, *12* (5), 398−404.
(52) Huber, G.; Mantz, H.; Spolenak, R.; Mecke, K.; Jacobs, K.; Gorb, S. N.; Arzt, E. Evidence for Capillarity Contributions to Gecko Adhesion from Single Spatula Nanomechanical Measurements. *Proc. Natl. Acad. Sci. U. S. A.* **2005**, *102* (45), 16293−16296.

DOI: 10.1021/acsami.5b07287
ACS Appl. Mater. Interfaces 2015, 7, 24127−24135

(53) Arzt, E.; Gorb, S.; Spolenak, R. From Micro to Nano Contacts in Biological Attachment Devices. *Proc. Natl. Acad. Sci. U. S. A.* **2003**, *100* (19), 10603−10606.
(54) Greiner, C.; del Campo, A.; Arzt, E. Adhesion of Bioinspired Micropatterned Surfaces: Effects of Pillar Radius, Aspect Ratio, and Preload. *Langmuir* **2007**, *23* (7), 3495−3502.
(55) P. V. GmbH Product database. https://www.piab.com/Products/suction-cups/shape/universal/u---universal-2-50-mm/ (accessed Sep 21, 2015).

DOI: 10.1021/acsami.5b07287
ACS Appl. Mater. Interfaces 2015, 7, 24127−24135